Giant Coulomb broadening and Raman lasing in ionic transitions

A. A. Apolonsky, S. A. Babin, A. I. Chernykh, S. I. Kablukov, S. V. Khorev, E. V. Podivilov, and D. A. Shapiro
Institute of Automation and Electrometry, Novosibirsk 630090, Russia
(Received 20 March 1996)

Continuous-wave generation of an anti-Stokes Raman laser on a number of blue-green argon-ion lines ($4p$-$4s$ and $4p$-$3d$) has been demonstrated with optical pumping from metastable levels $3d'\,^2G$ and $3d\,^4F$. It is found that the population transfer rate is increased by a factor of 3–5 (and hence the output power of the Raman laser) owing to Coulomb diffusion in the velocity space. The excitation and relaxation rates for the metastable level have been measured. The Bennett hole on the metastable level has been recorded using the probe field technique. It has been shown that Coulomb diffusion changes the shape of the contour to an exponential cusplike profile. Its width exceeds the Lorentzian one by 100 times and is close to the Doppler width. Such a giant broadening is also confirmed by the shape of the absorption saturation curve. [S1050-2947(96)02911-3]

PACS number(s): 42.55.Ye, 52.20.Hv, 32.70.Jz

I. INTRODUCTION

Stimulated Raman light scattering is widely used for frequency conversion of laser radiation [1]. In recent years there has been active development of cw anti-Stokes Raman lasers (ASRLs) with frequency up-conversion that use two-photon inversion in the active media of known lasers with gas-discharge excitation. cw generation of the ASRL has been successfully achieved for argon-ion [2] and He-Ne [3] laser media as well as for heavier noble atoms in electric discharge [4]. The conversion of radiation (648.3→437.5 nm) in a three-level Λ scheme was studied [2] for Ar II: $3d\,^2P_{3/2}\rightarrow 4p\,^2S^o_{1/2}\rightarrow 4s\,^2P_{3/2}$. In the level scheme employed, a stepwise process from the $3d$ metastable to the upper laser level $4p$ takes place with a subsequent emission on the $4p\rightarrow 4s$ transition. Despite the parameters of metastable level $3d\,^2P_{3/2}$ being not optimal (the radiative lifetime of about 30 ns [5,6] is comparable with the lifetimes of the $4p$ levels involved in laser transitions), the conversion efficiency appeared comparatively high. In particular, it was much higher than that in cw Raman lasers on atomic gases [3,4].

In the present paper, we study the factors that can enhance output parameters of a Raman laser based on ions in a gas-discharge plasma. In the comparatively dense and cold argon-laser plasma, the Coulomb ion-ion collisions [7] play the key role. Collisions accompanied by a change of velocity effectively increase the number of particles that interact strongly with the resonant radiation and the longer the level's lifetime the larger the possible increase in particle number. Estimations indicate that the width of the hole ''burnt'' in the velocity distribution for metastables with lifetimes $\geqslant 10^{-7}$ s should be comparable with the Doppler contour in width. This means that nearly all ions in the metastable state interact with radiation.

In order to study collisional effects we achieved Raman generation on a number of transitions in the Λ configuration $3d\rightarrow 4p\rightarrow 4s(3d)$ starting from the $3d'\,^2G$ and $3d\,^4F$ levels, which have almost no radiative decay [5,6]. However, it is a fact that the metastable level relaxation in Ar^+-laser plasma is determined by the deactivation due to ion-electron collisions [7]. The data for levels of interest are either unknown or there are contradictory data in different papers [8,9]. To carry out quantitative analysis, one has to measure both the excitation and deactivation rates of the metastable level under actual discharge conditions. In this paper, we report relatively high output parameters of Raman laser obtained without any optimization (even a plain linear cavity allowed the up-conversion efficiency of more than 50%, see Sec. II). Since the population transfer rate and hence the Raman laser output power rely upon the metastable level excitation rate and the part of the velocity distribution transferred to the upper level, we concentrated on the absorbing transition for a specific $3d'\,^2G_{7/2}$ level, aiming to clarify the role of collisions. We have studied the absorption saturation (Sec. III) and nonlinear resonance in the probe field scheme originated by the Bennett hole on the metastable level (Sec. IV). Both experiments show a giant broadening of the Bennett hole.

In addition, the relaxation and excitation rates for the metastable level were determined from the experimental data. We processed our data using formulas from [10], which are valid for the simple two-level model. We had modified them considering two aspects: the difference between magnetic sublevels and absorption of light in optically thick media. The formulas were checked against our numerical simulation (Sec. V), which included the deceleration due to dynamic friction force as well.

II. GENERATION OF THE ANTI-STOKES RAMAN LASER

In the present work, we have recorded the generation induced by optical pumping from the metastable to the upper laser level on a series of transitions (Table I). The schematic diagram of the experimental setup is presented in Fig. 1. We used the output of a single-frequency linearly polarized dye laser as the pump source. The pump radiation wavelength was controlled by a λ meter with a resolution of 10^{-3} nm. This was done using a fraction of the pump beam reflected by mirror M_1. The main beam was directed by mirror M_2

TABLE I. Anti-Stokes laser schemes in Ar II realized in the experiment. Schemes marked by asterisks are analogous to Ref. [2].

Pump → anti-Stokes lines (nm)	Levels	Remarks
610.4→457.9	$3d\,^2P_{1/2}\rightarrow 4p\,^2S^o_{1/2}\rightarrow 4s\,^2P_{1/2}$	*
648.3→457.9	$3d\,^2P_{3/2}\rightarrow 4p\,^2S^o_{1/2}\rightarrow 4s\,^2P_{1/2}$	*
613.9→496.5	$3d\,^4F_{5/2}\rightarrow 4p\,^2D^o_{3/2}\rightarrow 4s\,^2P_{3/2}$	
624.3→488.0	$3d\,^4F_{7/2}\rightarrow 4p\,^2D^o_{5/2}\rightarrow 4s\,^2P_{3/2}$	
617.2→501.7	$3d'\,^2G_{7/2}\rightarrow 4p'\,^2F^o_{5/2}\rightarrow 3d\,^2D_{3/2}$	

and further focused by lense L into the discharge tube. The cavity of the argon laser consisted of highly reflective mirror M_3 and output mirror M_4. Mirror M_3 had a high transmission in the red spectrum. In the absence of a pump beam, a usual series of well-known Ar II lines was observed. At transmission 5–10 % of mirror M_4 in the blue-green region, weak lines 457.9, 496.5, and 501.7 nm had low gain-to-loss ratios. Under such conditions, the fraction of the output power that came from the optical pump was substantially larger than the usual lasing. The output lines were separated by prism Pr. Aperture D_2 served to select the TEM_{00} mode of the argon laser and together with D_1 maintained the pump and Raman beams coaxiality, which greatly simplified alignment. In our experiments, we employed an argon-ion laser with a longitudinal gas flow in order to achieve high longitudinal uniformity of the discharge [11]. A 7-mm-bore discharge tube was 1 m in length; it operated at a current of 100 A, the pressure being set optimally for argon laser generation. These parameters were used throughout this work.

Transitions marked by an asterisk in Table I have the same starting levels as in [2]: $3d\,^2P_{1/2}$ and $3d\,^2P_{3/2}$. Using the 457.9-nm line instead of 437.5-nm line, which has a larger Einstein coefficient, we obtained a conversion efficiency (output power exceeded 30% of pump power) comparable to that of [2], already in a plain linear scheme of the Raman laser. Further, in the scheme with metastable states ^2G, ^4F, the efficiency was considerably higher (up to 60%).

For a detailed study, we chose the scheme with the largest pump radiation absorption ($3d'\,^2G_{7/2}\rightarrow 4p'\,^2F^o_{5/2}\rightarrow 3d\,^2D_{3/2}$); see Fig. 1. We measured the detuning of Raman laser with a scanning interferometer (5 GHz free spectral range) and a photodiode connected to an oscilloscope. In the absence of optical pumping, we observed generation on 501.7 nm near the threshold; the total gain under these conditions amounted to around 10%, only a narrow part of the gain contour near the line center being above the threshold. Note that a noise spectrum with a width of about 1 GHz was recorded with random jumps among adjacent laser modes. Under a single-frequency optical pumping on the 617.2-nm line an additional narrow peak of Raman generation appeared. The noisy background disappeared when the peak was tuned into the line center. When the pump power was 70 mW we observed that the Raman peak shift was consistent with the detuning of the pump radiation and was present in the output up to a detuning of ± 4 GHz. Even then, the gain coefficient induced by the optical pumping exceeded 10%. This result is important as it shows that the system can be optimized using multimirror cavities as described in [2] to produce a high output power with a wide detuning range.

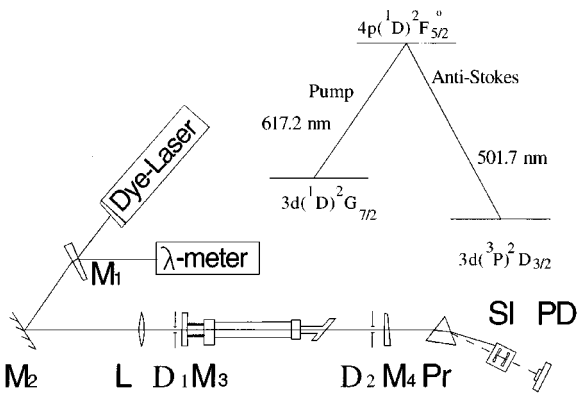

FIG. 1. Experimental setup for the study of Raman generation: M_1,M_2, beam turning mirrors; L, lens; D_1,D_2, aperture stops; M_3,M_4, argon laser cavity mirrors; Pr, dispersion prism; SI, scanning interferometer; PD, photodetector. There is a scheme of levels involved in Raman generation in this figure.

III. ABSORPTION SATURATION

For absorption measurement the scheme in Fig. 1 was used, except that mirror M_4 was removed and hence no generation occurred. Lens L was chosen so that the beam diverged only slightly along the discharge tube. The pump beam was attenuated with a set of filters and the transmitted intensity was registered. The power that came through was normalized to the average beam cross section $S=0.44\pm 0.05$ mm^2 and thus we obtained the average intensities I_i and I_f at the entrance to and the exit from the discharge tube, respectively.

The saturation behavior of absorbed power for ionic transitions is strongly dependent on diffusion in velocity space caused by Coulomb collisions [7,10]. The measured densities and temperatures are $N_i=N_e\simeq 1.7\times 10^{14}$ cm^{-3}, $T_i=m_i v_T^2/2\simeq 1$ eV, and $T_e\simeq 5$ eV. The effective frequency of ion-ion collisions amounts to $\nu_{ii}\simeq 2\times 10^7$ s^{-1} and so the diffusion coefficient is $D\simeq 5\times 10^{17}$ cm^2 s^{-3}:

$$\nu_{ii}=\frac{16\sqrt{\pi}N_i e^4\Lambda}{3m_i^2 v_T^3},\quad D=\frac{\nu_{ii}v_T^2}{2}, \tag{1}$$

where Λ is the Coulomb logarithm, e is the electron charge, and m_i is the ion mass. It is shown in [10] that whenever diffusion is strong, the absorbed power P per unit volume as a function of the field intensity $I=16\pi^2\hbar c|G|^2/\lambda^3 A_{mn}$ has the form

$$P=\frac{2\hbar\omega\sqrt{\pi}[N_n(g_m/g_n)-N_m]}{kv_T}\frac{|G|^2}{1+|G/G_s|^2}, \qquad (2)$$

$$|G_s|^2=\frac{\sqrt{2\nu_{ii}}kv_T}{2\pi}\left(\frac{1}{\sqrt{\Gamma_m}}+\frac{1}{\sqrt{\Gamma_n}}\right)^{-1}, \qquad (3)$$

with $|G|^2=|Ed_{mn}/2\hbar|^2$ the Rabi frequency. The diffusion width $kv_T\sqrt{\nu_{ii}/2\Gamma_j}$ enters in saturation parameter $|G_s|^2$ instead of the homogeneous width Γ_{mn}. Then the dependence $P(I_i)$ behaves as in the case of homogeneous saturation. The formula is valid up to the intensities satisfying the condition $kv_T\sqrt{\nu_{ii}/2\Gamma_n}\gg|G|\sqrt{\Gamma_{mn}/\Gamma_n}$. This means that the Coulomb broadening at metastable level exceeds the field broadening. The results of [10] were obtained with the assumption that

$$kv_T\gg\Gamma_n,\Gamma_m,\Gamma_{mn},\Omega, \quad \nu_{ii}(kv_T)^2/\Gamma_{mn}^3\ll1, \qquad (4)$$

where $\Omega=\omega-\omega_{mn}$ is the difference between the radiation frequency and the Bohr frequency of the m-n transition and Γ_j are the relaxation constants for the levels $\Gamma_{mn}=(\Gamma_m+\Gamma_n)/2$.

The above assumption appears well justified for the Ar II laser lines. In our case it is not valid since the metastable relaxation constant Γ_n is much less than those for the laser levels. Provided the radiation is linearly polarized, we can neglect the degeneracy and treat the $3d'^2G_{7/2}\rightarrow4p'^2F^o_{5/2}$ transition as a two-level system taking into consideration the degeneracy factors $g_{m,n}=2J_{m,n}+1$ of upper (m) and lower (n) levels. To check for validity of expressions (2) and (3) for concrete levels we compared them with a numerical solution of the equations for the density matrix (see Sec. V).

As long as up to 90% of the incident radiation is absorbed, it is necessary to consider the optical thickness of the medium. In such a case, the relation between the incident (I_i) and output (I_f) intensities is

$$\ln\left(\frac{I_i}{I_f}\right)+\frac{I_i-I_f}{I_s}=k_0l, \qquad (5)$$

with the small-signal absorption coefficient in the standard form

$$k_0\simeq\frac{\lambda^3A_{mn}}{8\pi^{3/2}v_T}\left(N_n\frac{g_m}{g_n}-N_m\right) \qquad (6)$$

and the saturation intensity being

$$I_s=\frac{8\pi\sqrt{2\nu_{ii}}kv_T\hbar c}{\lambda^3A_{mn}}\left(\frac{1}{\sqrt{\Gamma_m}}+\frac{1}{\sqrt{\Gamma_n}}\right)^{-1}. \qquad (7)$$

In Fig. 2 the dependence of the absorption $\Delta I=I_i-I_f$ on the incident intensity I_i given by expression (5) is plotted along with the experimental points using the maximum-likelihood fitting. The unsaturated absorption coefficient k_0 has an experimental value of $(2.14\pm0.05)\times10^{-2}$ cm^{-1}, while the saturation intensity I_s was measured to be 11.2 ± 2.1 W/cm^2. A comparison between the absorption on this transition and the gain coefficient for an adjacent transition 501.7 nm indicated that the population of metastable level $3d'^2G_{7/2}$ was 14 times that of $4p'^2F^o_{5/2}$. Knowing the Einstein coefficient for this transition $A_{mn}=2.2\times10^7$ s^{-1} [6] and the discharge length $l=100$ cm, one can obtain the lower level population $N_n\simeq(5.33\pm0.14)\times10^{10}$ cm^{-3} from formula (6). One can also determine the lower level decay rate with the help of Eq. (7). The upper level decay rate was taken from the literature: $\Gamma_m=2.0\times10^8$ s^{-1} ($\tau_m=8.4$ ns is the radiative lifetime [6] and $K_m\simeq10^{-7}$ cm^3 s^{-1} is the deactivation constant [12]).

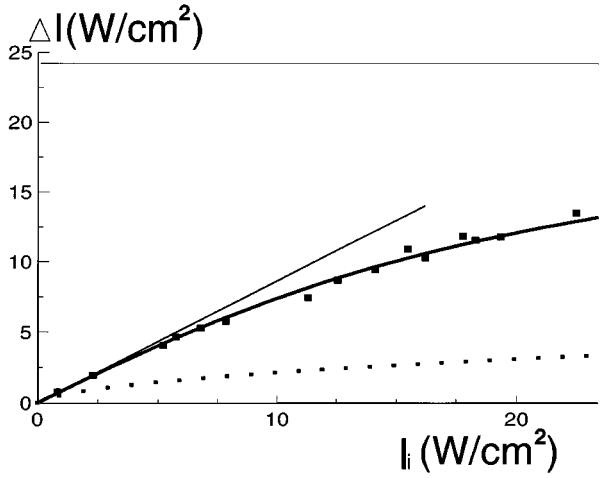

FIG. 2. Dependence of the absorbed intensity $\Delta I=I_i-I_f$ on the transition $3d'^2G_{7/2}\rightarrow4p'^2F^o_{5/2}$ upon the incident intensity I_i. Boxes correspond to experimental data. The theoretical dependence (solid curve) (5) is fitted with the maximum-likelihood algorithm. Dots correspond to inhomogeneous saturation with Coulomb diffusion neglected. The straight lines correspond to the slope of the saturation curve at zero intensities and to the asymptote of maximum possible absorption.

The lifetime obtained for lower level is $\Gamma_n\simeq(7.7\pm4.6)\times10^7$ s^{-1}. The accuracy is low as only slight saturation was achieved. Additional error has been introduced by the uncertainty in the measured saturation intensity associated with nonuniformity of the beam. Since the expression for Γ_n includes a difference of two close values, the calculated result should be viewed as an estimation. By measuring the width of the nonlinear resonance in the spectrum of the probe field one can determine more accurately the metastable level relaxation constant. As soon as the contribution of levels m and n into the nonlinear resonance is inversely proportional to Γ_j, one can say, on the basis of the results, that the contribution of the lower level is at least 3 times greater than that of the upper one. The measurement of the nonlinear resonance shapes are covered in the next section.

IV. NONLINEAR RESONANCE

The scheme of the experiment to measure the nonlinear resonance in the probe field spectrum is presented in Fig. 3. To split the dye laser beam into two, the pump beam and the probe one (a and b in Fig. 3, respectively), we used reflection from the uncoated surface of the output mirror (M_1 in Fig. 3). The probe beam power amounted to a few percent of the power of the strong beam. Lenses L_1 and L_2 were used to

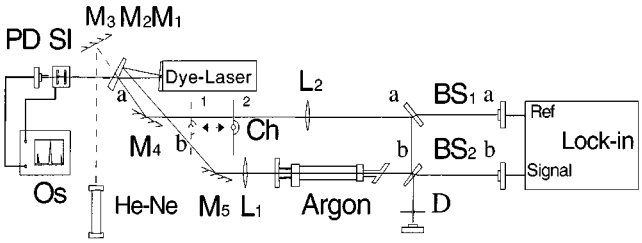

FIG. 3. Experimental setup for the study of the nonlinear resonance in the probe field configuration: M_1, coupling mirror of dye laser; M_2, M_3, M_4, M_5, beam turning mirrors, BS_1,BS_2, beam splitters; L_1, L_2, focusing lenses; Ch, beam chopper; D, small aperture stop. *a* and *b* mark pump and probe beam paths, respectively. The chopper in position 1 modulates both pump and probe fields; in position 2 it affects only the pump beam. The scanning interferometer (SI), photodetector (PD), oscilloscope (OS), and single-frequency He-Ne laser are the components of the spectrum analyzer.

ensure minimal divergence of the beams along the discharge tube, the diameter of the probe beam being 3 times smaller than that of the pump beam. The probe beam that passed through the discharge was detected behind the beam splitter BS_2 (transmission $t \sim 20\%$). The lock-in detector Unipan 232B was used. A fraction of the pump beam coming through the splitter BS_1 and modulated by the chopper was used as the reference signal. The chopper in position 1 modulates both beams and the lock-in detector registers the power of the probe beam transferred through the discharge. When placed in position 2, the chopper influences the pump beam only and the lock-in detector registers the variation of the transferred power due to the influence of the pump beam. The intensity of the pump field was measured taking into account the variation of the dye laser beam crossection. For this purpose, the intensity near the beam axis was registered using an aperture stop D (with a diameter much smaller than the effective beam diameter). The detuning was measured with a scanning interferometer, photodiode, and oscilloscope. Along with the dye laser frequency, the scanning interferometer registered the single-frequency He-Ne laser signal. The latter served as a reference point to detuning of the dye laser.

Owing to a strong absorption, the depth of the burnt Bennett hole changes along the discharge. Consequently, we require a formula for the resonance in an optically thick medium. Neglecting the influence of the probe field I_1 on the strong one I_2, which propagates in the opposite direction from the point $z=l$ to 0, we have an exponential intensity dependence on the distance z: $I_2(z)=I_2(l)\exp[k(\Omega_2)(z-l)]$. The corresponding dependence of the weak field intensity $I_1(z)$ can be extracted from the following equation, taking into account a weak saturation of the transition by the strong field $I_2(z)$:

$$\frac{dI_1(z)}{dz} = -k(\Omega_1)I_1(z)\left(1 - F(\Omega_1,\Omega_2)\frac{I_2(z)}{I_s}\right), \qquad (8)$$

where $\Omega_{1,2}$ are the frequency detunings of the weak and strong fields from the exact resonance respectively;

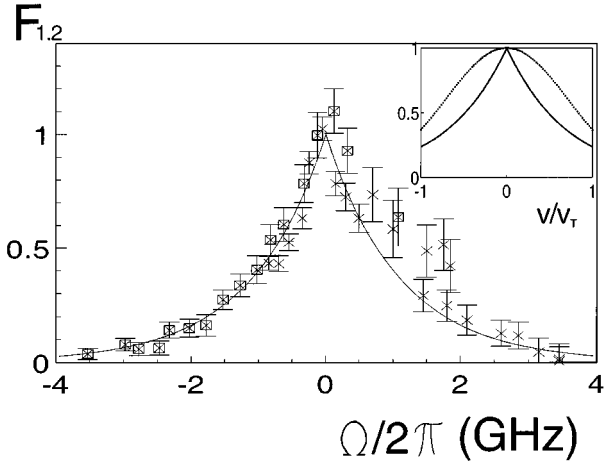

FIG. 4. Function (10) $F_{1,2}$ versus detuning $\Omega/2\pi$ (in GHz) fitted into the experimental points. Crosses and boxes denote two different data sets. For comparison, the Doppler velocity distribution (in v_T units) and the shape of the Bennett hole on the metastable level are also shown.

$$F(\Omega_1,\Omega_2) \simeq \exp\left(-\frac{|\Omega_2-\Omega_1|}{kv_T}\sqrt{\frac{2\Gamma_n}{\nu_{ii}}}\right), \qquad (9)$$

where F is the function that describes the shape of the Bennett hole in the case of diffusion broadening (see [7] and references therein; the validity of the expression as applied to the studied transition is discussed in Sec. V). In the scheme under investigation $\Omega_1 = -\Omega_2 = \Omega$, thus the velocities of the particles resonant to the probe and pump field $\pm\Omega/k$ differ only in sign.

The solution of Eq. (8) can be written in the form

$$F_{1,2} = F(\Omega,-\Omega) \simeq \frac{I_s[I_1(l)-\tilde{I}_1(l)]}{I_2(l)\tilde{I}_1(0)\{1-\exp[-k(\Omega)l]\}\exp[-k(\Omega)l]}, \qquad (10)$$

where $\tilde{I}_1(l)=\tilde{I}_1(0)\exp[-k(\Omega)l]$ is the probe field intensity in the absence of the strong field, i.e., at $I_2=0$.

In the experiments, the readings of the lock-in detector were recorded when the chopper was in position 2; in this case they were proportional to $I_1(l)-\tilde{I}_1(l)$. The input intensities of the probe $\tilde{I}_1(0)$ and pump $I_2(l)$ fields were proportional to the output power of the dye laser. With the chopper in position 1 we measured the dependence of the absorption coefficient upon detuning $k(\Omega)=k_0\exp[-\Omega^2/(kv_T)^2]$. From these data we reconstructed $F_{1,2}$ as a function of detuning Ω up to an arbitrary amplitude.

The dependence determined in this way is demonstrated in Fig. 4. It is relevant to mention that the experimental data consist of two overlapping sets of points because it was difficult to cover the required range in one sweep. Experimental points were approximated by expression (9) using a maximum-likelihood fitting. Three parameters were fitted: magnitude, width, and detuning zero shift. The processed data yielded diffusion width $\Delta=(\ln 2/\pi)\sqrt{\nu_{ii}/2\Gamma_n}kv_T=3.0\pm0.3$ GHz, the Doppler width

being $\Delta\nu_D = kv_T\sqrt{\ln 2}/\pi = 5.3 \pm 0.1$ GHz. Internal noises of the dye laser in the vicinity of the strong-field chopping frequency can lead to a systematic error, that is, the total error can exceed 10%. The decay rate of the metastable level determined from the diffusion width is $\Gamma_n = (2.3 \pm 0.5) \times 10^7$ s^{-1}, which agrees with the value obtained from the saturation intensity. Hence our assumptions concerning the contributions of the upper and lower levels into the resulting contour of the nonlinear resonance are obviously true, $\Gamma_n \simeq 0.1\Gamma_m$. To compare the Bennett hole width and that of the Doppler contour, we show the respective velocity distributions at zero detuning from exact resonance in the inset to Fig. 4. We should take into account that the Bennett hole full width at half a maximum is Δ and the width of function $F_{1,2}$ in Eq. (9) and Fig. 4 is $\Delta/2$, which comes from scanning the hole with double speed. It is seen from the plot that collisions ''blur'' the Bennett hole to almost whole Doppler contour. In addition, knowing the relaxation rate and population we find the excitation rate of the metastable level Q_n to be 1.6 times greater than that of the upper laser level.

V. NUMERICAL SIMULATION

Not all the assumptions of [10] were valid for our investigation; we needed to check the accuracy of analytical calculations. To this end, we solved numerically the equations for the density matrix of a two-level system in the field of a running electromagnetic wave, including the Coulomb diffusion and the dynamic friction force. These equations are as [7]

$$\begin{aligned}(\Gamma_{mn} - i\Omega + ikv)\rho_{mn} - \hat{D}\rho_{mn} &= -iG(\rho_{mm} - \rho_{nn}),\\ \Gamma_m\rho_{mm} - \hat{D}\rho_{mm} &= Q_m W(v) - 2\mathrm{Re}(iG^*\rho_{mn}),\\ \Gamma_n\rho_{nn} - \hat{D}\rho_{nn} &= Q_n W(v) + 2\mathrm{Re}(iG^*\rho_{mn}),\end{aligned} \tag{11}$$

where

$$\hat{D}\rho_{ij} = \nu_{ii}\frac{\partial}{\partial v}\left[v\rho_{ij} + \frac{v_T^2}{2}\frac{\partial\rho_{ij}}{\partial v}\right], \tag{12}$$

Q_j is the total excitation rate of the jth level, and $W(v)$ is the one-dimensional Maxwell distribution over velocity having width v_T. The terms proportional to A_{mn} have been neglected since they are small for the transition in question, $A_{mn} \simeq 0.1\Gamma_m$. For numerical solution of Eq. (11) the symmetrical differences in operator $\hat{D}$ were substituted for partial velocity derivatives. At $v = 5v_T$ we took the asymptotic condition $\rho = 0$ and solved the resulting array of linear algebraic equations using the matrix sweep method. To calculate the field work and the shape of the nonlinear resonance, we averaged the distribution for $\rho_{ij}(v)$ over velocity, using the formalism given in [7].

A different behavior of the magnetic sublevels was taken into consideration too. When a linearly polarized field interacts with transition $3d'^2G_{7/2} \rightarrow 4p'^2F^o_{5/2}$, the only allowed transitions are those conserving the projection M of angular momentum J onto the polarization direction. Magnetic sublevels with the same projection M can be regarded as independent two-level subsystems with different dipole moments

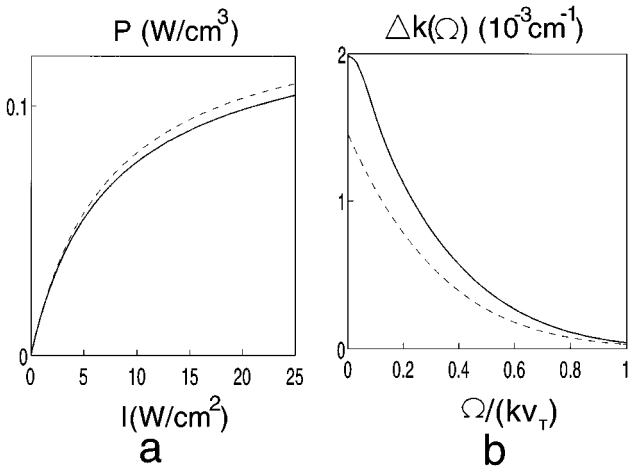

FIG. 5. (a) Dependence of the absorbed power P upon field intensity I in an optically thin medium for a two-level system (2) and a numerical simulation (11) for magnetic sublevels with friction force included (dashed and solid curves, respectively). (b) Variation of the absorption coefficient $\Delta k(\Omega) = F_{1,2}\exp[-\Omega^2/(kv_T)^2]I_2/I_s$ caused by the strong field at the intensity $I_2 = 0.1I_s$: the solid curve plots the results of numerical simulation and the dashed curve is the analytical approximation (parameters are taken from experiments).

$$|d_M|^2 = |\langle m||d||n\rangle|^2 \left| \begin{pmatrix} 7/2 & 5/2 & 1 \\ M & -M & 0 \end{pmatrix} \right|^2, \tag{13}$$

where $\langle m||d||n\rangle$ is the normalized dipole moment,

$$|d_{5/2}|^2 = \frac{3}{28}\frac{|\langle m||d||n\rangle|^2}{3}, \quad |d_{3/2}|^2 = \frac{5}{28}\frac{|\langle m||d||n\rangle|^2}{3},$$
$$|d_{1/2}|^2 = \frac{3}{14}\frac{|\langle m||d||n\rangle|^2}{3}. \tag{14}$$

At a given intensity I, the field magnitude (in frequency units) $|G_M|^2 = |Ed_M/2\hbar|^2$ is different for every subsystem. The absorbed power is found by summing up over all subsystems. For each of them expression (2) is valid with the substitutions $|G|^2 \rightarrow |G_M|^2$ and $[(g_m/g_n)N_n - N_m] \rightarrow [(N_n/g_n) - (N_m/g_m)]$. At low and high intensities $I \ll I_s$ and $I \gg I_s$, the total absorption is exactly the same as that of a two-level system according to Eq. (2). The largest deviation is achieved at $I = I_s$ and does not exceed 2%.

Unknown constants in (11) were taken from independent measurements. The population of the metastable level was obtained in the experiments on absorption saturation. The upper level population was given by the measurements of the gain coefficient on the adjacent laser transition. The decay rate of metastable level was taken from experiment with nonlinear resonance in the probe field spectrum.

Figure 5(a) displays the dependence of absorbed power P per unit volume upon field intensity I_i for a two-level system in an optically thin medium. Theoretical values calculated from Eq. (2) (dotted line) are shown along with those obtained numerically including the dynamic friction and degeneracy (solid curve).

One can see from Fig. 5(a) that the difference between the two curves is within 5%. This shows that the discrepancy mainly results from the dynamic friction. Also, the numerical data at given values $\Gamma_j, Q_j, A_{mn}, \nu_{ii}, v_T$ can be shown to agree with the function $P(I)=k_0 I/(1+I/I_s)$, but with different values for k_0 and I_s. Those values are lower by 2% and 6%, respectively, than k_0 and I_s in (6) and (7).

The contour of the nonlinear resonance $\Delta k(\Omega)$ was calculated numerically for the intensity of the strong field $I_2=0.1I_s$ and the probe field intensity $I_1 \ll I_s$ according to the experimental conditions. In Fig. 5(b), the solid curve stands for numerical calculations and the dashed line corresponds to the analytical approximation $\Delta k(\Omega) = F_{1,2}\exp[-\Omega^2/(kv_T)^2]I_2/I_s$ used for processing the experimental data. It deviates from the numerical simulation by a factor of 1.45 with an accuracy not worse than 3% over the whole detuning range, i.e., it closely follows the shape of the resonance.

VI. DISCUSSION

We analyzed the dependence of absorption upon pump field intensity, as well as the nonlinear resonance that comes from the Bennett hole on the metastable level. This included an approximation of the experimental values with analytical expression and a comparison of the theory with numerical solutions of the equations for the density matrix. As a result, it was clearly demonstrated that the unusual features of both the saturation curve and the Bennett hole are primarily due to the Coulomb diffusion of ions in the velocity space. The diffusion leads to an abnormal broadening of the Bennett hole: the diffusion width of the hole Δ for the metastable $3d'^2G_{7/2}$ reaches 3 GHz, whereas the Lorentzian width of the transition Γ_{mn}/π amounts to as little as 35 MHz. The relative broadening is thus nearly by a factor of 100. With the field broadening included, the transition width $\Gamma_{mn}\sqrt{1+4|G|^2/\Gamma_m\Gamma_n} \sim 10\Gamma_{mn}$ is also much less than the diffusion one. Thus the giant Coulomb broadening completely determines the shape of saturation curve for the transition.

Instead of the well-known ''hole burning'' in the velocity distribution, one observes nearly complete saturation of the whole Doppler contour. The shape of the nonlinear resonance has an unusual exponential cusp (see Fig. 4). Note that such exponential wings were observed in the spectrum of the probe field on transition $3d'^2G_{9/2} \rightarrow 4p'^2F_{7/2}$ of argon ion under conditions of hollow cathode discharge [9,13]. The authors of those papers attributed the broadening to ion-atom collisions. Since plasma parameters were not measured, quantitative analysis is difficult. However, despite considerable difference in plasma parameters (specifically, much lower charged particle concentrations in hollow cathode), Coulomb collisions may also play a noticeable role there.

Coulomb broadening changes the saturation curve very much. The inhomogeneous saturation $k_0/\sqrt{1+|G|^2/|G_0|^2}$, which is typical for single-frequency pumping, is replaced by homogeneous saturation $k_0/(1+|G|^2/|G_s|^2)$. The saturation intensity differs by a factor of 60 for these cases. The dotted line in Fig. 2 corresponds to inhomogeneous saturation and the horizontal line is the greatest possible absorbed power $P \simeq (6/8)Q_n\hbar\omega Sl$ (the expression is valid for $\Gamma_n \ll \Gamma_m$). At intensities attained in our experiments, the curve that takes Coulomb diffusion into account is saturated noticeably as it draws near the asymptotic value, whereas the inhomogeneous saturation curve is not saturated at all. At pump intensities $I \sim I_s$ diffusion causes the absorption (and with it the output power of the Raman laser on the adjacent transition) to increase by a factor 3–5 depending on the values of relaxation constants. Note that the perturbation influence of Raman generation on absorption of the pump radiation is small when $\Gamma_n \ll \Gamma_m$. At low intensities (much lower than the saturation intensity on the adjacent transition) the generation follows the dependence of absorbed power on the pump input. We should mention that simple expressions for the output power of an ionic Raman laser have been derived earlier [14] by the perturbation method for low pump and generation intensities.

Let us compare the value obtained for the relaxation constant of the metastable level $\Gamma_n \simeq 2\times10^7\ \mathrm{s}^{-1}$ with some data found in other papers. We know no published data for level $3d'^2G_{7/2}$ deactivation in plasma. However, there are some results on the similar metastable level $3d'^2G_{9/2}$. In [8], the laser induced fluorescence was observed in a hollow cathode discharge. The measured electron deactivation coefficient appeared to be $(2.5\pm1.0)\times10^{-8}\ \mathrm{cm}^3/\mathrm{s}$, the electron temperature being $T_e=3.5$ eV. For electron density $N_e \simeq 2\times10^{14}\ \mathrm{cm}^{-3}$, which is relevant to our experiments, we get the decay rate $\Gamma_n \sim 5\times10^6\ \mathrm{s}^{-1}$. The relaxation constant of the metastable level $3d'^2G_{9/2}$ $\Gamma_n \sim 10^8\ \mathrm{s}^{-1}$ is found in [9], again for a hollow cathode discharge. Authors of Ref. [9] hypothesized that metastable is quenched due to resonant charge-exchange collisions of excited argon ions with atoms in the ground state. The estimation for the electron deactivation of level $3d'^2G_{7/2}$ done in Bates-Damgaard approximation (using tables in [15]) yields $\Gamma_n \simeq 4\times10^6\ \mathrm{s}^{-1}$, which is slightly lower than the measured value. This were done taking into account only the predominant channel $3d'^2G_{7/2} \rightarrow 4p'^2F^o_{5/2}$. It is likely that in our conditions relaxation occurred due to both collisions with electrons and resonant charge-exchange with neutral atoms. Consequently, the experimental value for the relaxation rate $\Gamma_n \simeq 2\times10^7\ \mathrm{s}^{-1}$ of level $3d'^2G_{7/2}$ does not contradict the estimation and differs from data given in [8,9] for $3d'^2G_{9/2}$ no more than they differ from each other.

Note that the metastable level we have studied has a relaxation rate comparable with the ion-ion collision frequency. Under such conditions the dynamic friction force and velocity dependence of the diffusion coefficient should lead to a noticeable narrowing of the Bennett hole centered on a far wing of the velocity distribution $|v| > v_T$ [16]. Experiments with independently tuned strong and probe fields could check this phenomenon.

VII. CONCLUSION

The present work has demonstrated the possibility of Raman generation due to an optical pumping from metastable levels $3d'^2G$ and $3d^4F$ on a number of generation lines of an argon laser. For the absorbing transition $3d'^2G_{7/2} \rightarrow 4p'^2F^o_{5/2}$ of the Raman laser 617.2→501.7 nm, the unsaturated absorption coefficient $k_0=2\times10^{-2}\ \mathrm{cm}^{-1}$ and saturation intensity $I_s=11\ \mathrm{W/cm}^2$ have been deter-

mined. The ratios of populations (~ 14) and excitation rates (~ 1.6) for levels $3d'^2G_{7/2}$ and $4p'^2F^o_{5/2}$ have been measured. The relaxation rate of level $3d'^2G_{7/2}$ is $\Gamma_n = 2.3\times 10^7$ s^{-1}. It is determined primarily by collisional deactivation in plasma. The Bennett hole on metastable level $3d'^2G_{7/2}$ is broadened by a factor of 100 owing to Coulomb collisions. The hole has an exponential shape and its width $\Delta \sim 3$ GHz is comparable with the Doppler one. This giant broadening is the key factor that influences the shape of saturation curve for the transition. Instead of usual hole burning in the velocity distribution, we observed an almost complete saturation of the whole Doppler contour. This increases the population transfer to the upper level and enhances the efficiency of the Raman laser.

ACKNOWLEDGMENTS

The authors are grateful to S. M. Kobtsev for technical assistance, to E. A. Yukov for a fruitful discussion of the kinetics of electron deactivation, and A. Shafarenko for his assistance in translation. This work has been partially sponsored by the International Science Foundation and the Russian Government, Grant No. RCN 300.

[1] J.C. White, Top. Appl. Phys. **59**, 115 (1989).
[2] A. Feitish, D. Schnier, T. Müller, and B. Wellegehausen, IEEE J. Quantum Electron. **24**, 507 (1988); B. Wellegehausen (unpublished).
[3] K. Rittner, A. Höpe, T. Müller-Wirts, and B. Wellegehausen, IEEE J. Quantum Electron. **28**, 342 (1992).
[4] K. Rittner, A. Wicht, G. Jordan, A. Heuer, H. Welling, and B. Wellegehausen, Laser Phys. **4**, 339 (1994).
[5] B.F. Luyken, Physica **60**, 432 (1972).
[6] A. Hibber and J. Hansen, J. Phys. B **27**, 3325 (1994).
[7] S.A. Babin and D.A. Shapiro, Phys. Rep. **241**, 119 (1994).
[8] H.M.I. Willems, K. Yuasa, B. van der Sijde, D.C. Schram, and J.A.M. van der Mullen, J. Quant. Spectrosc. Radiat. Transfer **41**, 251 (1989).
[9] M. Elbel, M. Simon, and H. Welp, Quantum Opt. **2**, 351 (1990).
[10] K.B. Kurlayev and D.A. Shapiro, Kvant. Elektron. **21**, 1080 (1994) [Sov. J. Quantum Electron. **24**, 1003 (1994)].
[11] S.A. Babin and A.E. Kuklin, Proc. SPIE **1397**, 589 (1991).
[12] J. Jolly, J. Quant. Spectrosc. Radiat. Transfer. **20**, 503 (1978).
[13] W. Bestgen, M. Elbel, R. Lange, and H. Welp, J. Phys. B **28**, 2575 (1995).
[14] S.A. Babin, S.G. Rautian, and D.A. Shapiro, Kvant. Elektron. **19**, 1139 (1992) [Sov. J. Quantum Electron. **22**, 1065 (1992)].
[15] I.I. Sobelman, L.A. Vainshtein, and E.A. Yukov, *Excitation of Atoms and Broadening of Spectral Lines* (Springer, Berlin, 1981).
[16] E.V. Podivilov, D.A. Shapiro, and M.G. Stepanov, Phys. Rev. Lett. **72**, 3979 (1995).